Improved Near-Field Transducer Design for Heat-Assisted Magnetic Recording

Anurup Datta and Xianfan Xu

Birck Nanotechnology Center, School of Mechanical Engineering, Purdue University, West Lafayette, IN 47907 USA

Heat-assisted magnetic recording (HAMR) is the next-generation data storage technology that can address the challenge of increasing data storage capacity. The key to the design of an HAMR system is the near-field transducer (NFT) that focuses light to a very small scale in the range of tens of nanometers with a very high intensity. This is also associated with unwanted self-heating of the NFT, which is detrimental to the functionality of the NFT, and hence there is a need to improve NFT designs. We investigate a third dimension in the typical planer NFT design by introducing a taper in the model of an E antenna NFT design and study its effect on the optical and thermal performances of the NFT. We find that the proper optimization of the taper geometry gives rise to improved operation of the NFT. In addition, in terms of thermal figures of merit, its performance is also significantly superior.

Index Terms— **Heat-assisted magnetic recording (HAMR), near-field transducer (NFT).**

I. Introduction

ACCORDING to International Data Corporation, the total volume of global digital data is increasing by 40% annually and is estimated to reach 44 ZB or 44 trillion gigabytes by 2020; however, the world's amount of available storage capacity is growing at a much slower rate [1]. Thus, there is a continuous demand for the increase in data storage capacity, and in order to achieve a targeted value of areal data storage density of 1 Tb/in^2 and beyond, it is anticipated that heat-assisted magnetic recording (HAMR) will be a key technology in the next-generation hard disk drives (HDDs) [2]–[4]. HAMR exploits the optical near-field capabilities of a plasmonic nanostructure that enables localized heating of the recording medium in an HDD within a subdiffraction limited domain. The plasmonic antenna, also known as a near-field transducer (NFT), when excited with its working wavelength of light, can generate field intensity on orders of magnitude higher than the incident field intensity over an area of tens of nanometers [5], [6]. This gives rise to intense heating of the recording medium that is typically placed at a gap of a few nanometers from the antenna. The recording medium is typically made up of a high anisotropic magnetic medium, which helps to overcome the fundamental superparamagnetic limit [7]. Due to the localized heating of the recording medium, its coercivity decreases and makes it possible to address individually very small grain sizes in the recording medium in the presence of a magnetic field.

The performance of the HAMR system significantly depends on the design and material properties of the NFT. For achieving a high areal data storage density, on one hand, the NFT should be able to generate a high-intensity hot spot over a very small region. This is achieved by several approaches including: 1) making the structure resonant at particular wavelength; 2) introducing sharp tiplike features in the design thereby utilizing the "lightning rod" effect; and 3) by efficient use of an image dipole [8]. Some functional NFT designs include the triangular antenna [8], E antenna [9], lollipop structure [10], bowtie antenna [11], C-aperture [12], and nanobeak antenna [13]. Increasing the efficiency of the coupling of the incident laser power to the recording medium is one of the primary goals in designing a better NFT, which can be achieved by better impedance matching of the NFT with recording medium [14]. At the same time, the material of the NFT plays an equally important role in determining its functionality and reliability. In the optical wavelength range, metals that typically act as plasmonic materials are inherently lossy, causing heat to be generated in the metals itself, which could raise its temperature by several hundreds of degrees. This could cause several unwanted effects on the performance of the HAMR system such as expansion of the NFT head, failure of the NFT due to thermal stress, and failure of the interface materials [15]. As of now, gold has been the most preferred choice as the NFT material due to its plasmonic behavior at the near infrared range, its high thermal conductivity, and low corrosivity.

One of the methods to reduce the temperature rise within the NFT is to employ heat sink near the vicinity of the NFT. For this purpose, generally, the media stack contains a heat sink layer beneath the recording medium, which helps in dissipating heat away from the NFT as well as helping to minimize the spreading of heat within the recording medium [13]. Increasing heat conduction of the NFT also facilitates in reducing the temperature rise of the NFT. As such, by altering the shape of the lollipop antenna, a fat NFT was proposed [16]. However, the modified structure delivered a poorly confined hotspot [16], and hence further modifications were required for optimizing the performance of the NFT.

In this paper, we explore the improvement of the designs of the NFT in order to improve both the optical and thermal performances of the HAMR system. We specifically look at the effect of the third dimension in the normal planer NFT design, by simply introducing tapers in the notch of the E antenna to help in the reduction of the temperature rise of the NFT as well

Manuscript received May 19, 2016; revised June 27, 2016; accepted July 21, 2016. Date of publication July 27, 2016; date of current version November 16, 2016. Corresponding author: X. Xu (e-mail: xxu@ecn.purdue.edu).

Color versions of one or more of the figures in this paper are available online at http://ieeexplore.ieee.org.

Digital Object Identifier 10.1109/TMAG.2016.2595496

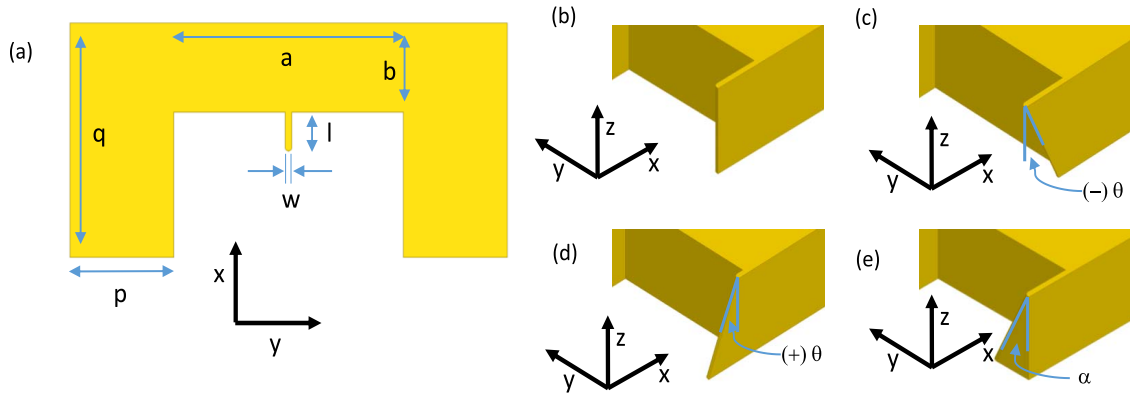

Fig. 1. (a) Top view of an E antenna with straight notch. Cross-sectional zoomed-in isometric views of the NFTs with different notch geometries for the (b) standard E antenna with notch having straight side walls, (c) E antenna with notch wall tapered outside along the x-direction, (d) E antenna with notch wall tapered inside along the x-direction, and (e) E antenna with notch wall tapered along the y-direction. In (b)–(e), the cross section was taken along the symmetric x–z plane.

as increased optical power delivery to the recording medium. Several geometrical configurations of the notch based on the taper angle are investigated, and the optical performances of these different designs in the presence of a recording medium are studied. Further, we carry out thermal simulations to study the temperature rise in the NFTs as well as the recording medium and evaluate the performance of the modified NFT geometries. We compare several thermal figures of merits for this purpose and show that by introducing an appropriate geometry in the notch of an E antenna, it is possible to significantly improve the thermal functionality of the NFTs.

II. Proposed NFT Geometry

It has been previously demonstrated that in the case of bowtie apertures as a plasmonic antenna, having a tapered side wall in place of a straight wall results in a higher field concentration and a sub-20-nm spot size [17]. In order to potentially improve the performance of the E antenna as an NFT, we introduce tapers in several configurations in order to increase the field concentration at the tip of the notch. Fig. 1(a) and (b) shows the isometric view and the cross-sectional side view, respectively, of an E antenna with a straight walled notch, which was demonstrated previously [9]. Fig. 1(c) shows the cross-sectional view of an NFT derived from the E antenna having a taper in the notch outward along the x-axis, which is denoted by the angle θ, which we call as negative θ. Fig. 1(d) shows a similar taper, but pointing inward along the x-axis, which is also denoted by the angle θ, called as positive θ. Fig. 1(e) shows a taper along the y-direction, denoted by the angle α, which gives rise to a notch having a wider base at the bottom than at the top. In the consecutive sections, the electromagnetic and thermal simulation models are described along with the different figures of merit and the optical and thermal performances of each of these different configurations are studied.

III. Simulation Models

A. Electromagnetic Simulation Model

Full wave 3-D numerical simulations were performed by commercial FEM-based software, ANSYS HFSS. The dimensions of the E antenna with the straight notch, as illustrated in Fig. 1(a), are as follows: body dimensions ($a = 316$ nm, $b = 114$ nm), wing dimensions ($p = 142$ nm, $q = 300$ nm), and the notch dimensions at the air bearing slider (ABS) side ($l = 50$ nm, $w = 12$ nm). The E antenna of thickness 85 nm is considered to be embedded in a glass substrate. Different layers of the recording media stack are considered to be present above the ABS. The ABS of the antenna is coated with a head overcoat (2.5 nm) to minimize corrosion and a lubricant (1 nm) to reduce friction. The air gap is assumed to be 2.5 nm. The media stack consists of a medium overcoat layer (2.5 nm), the storage medium (10 nm), and the interlayer (15 nm), which connects the heat sink layer (100 nm) to the media storage layer. A schematic setup of the simulation model is given in Fig. 2. Absorbing radiation boundary conditions are assumed at the outer surfaces of the simulation. A Gaussian beam of a 300-nm spot size polarized along the longitudinal axis of the notch, which is the x-axis in Fig. 1, is assumed to be incident on the NFT. The optical properties of gold are taken from [18] and the simulation is performed for wavelength of 800 nm.

B. Thermal Simulation Model

Based on the results of the electromagnetic simulations, thermal simulations are also performed to evaluate the thermal performance of the NFTs with tapers. Transient thermal simulations are implemented using ANSYS workbench, which is also an FEM-based modeling technique. The geometric model is imported into the workbench environment from the ANSYS HFSS simulation. The energy absorbed in the recording medium and the NFT is modeled as a heat generation term in the thermal simulation. The incident laser power is assumed to be 10 mW. It is assumed that the NFT is being heated constantly by the incident laser. The medium, however, is heated only for a short period of time due to the fast rotation. In addition, it has been proposed that operating the laser in pulsed mode in HAMR systems sometimes can be advantageous in terms of reducing the transducer temperature rise and producing a more confined heat area [19], [20]. Here, the medium is assumed to be heated

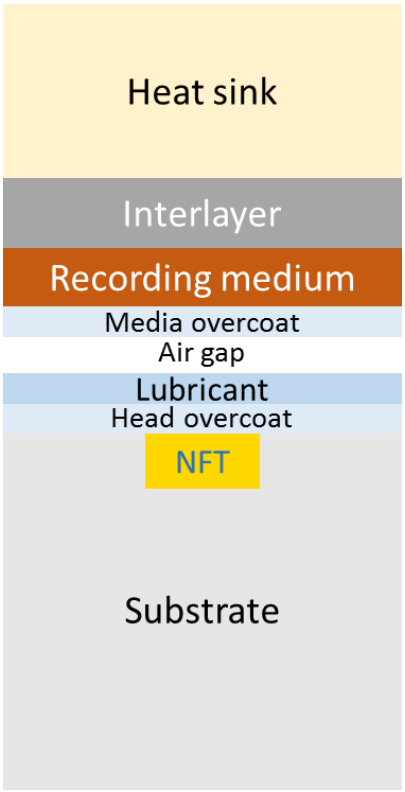

Fig. 2. Schematic of the recording media stack and the NFT embedded in the substrate.

for 1 ns, which corresponds to a linear speed of 50 m/s of the recording medium for a nominal heated spot size of 50 nm. Considering the effect of high air bearing pressure and very small head disk gap, the convection heat transfer coefficient in the air gap between the head and the recording medium was high [21], [22] and a representative value of 0.17 MW/m^{2}K was used as in [22]. However, it has been assessed that "the convection heat transfer does not play a significant role in the temperature distribution for heat transfer coefficients less than 10^8 W/m^{2}K [23]."

IV. Figures of Merit

A. Optical Figure of Merit

An appropriate figure of merit for quantifying the optical performance of the NFTs is the optical coupling efficiency, which is defined as the power absorbed in the recording medium in a volume defined by a cylinder of diameter 80 nm and height equal to the thickness of the recording medium divided by the net incident power. The power absorbed per unit volume is calculated according to

$$q''' = \frac{1}{2}\varepsilon_0 \omega \mathrm{Im}(\varepsilon)|E|^2 \quad (1)$$

where ε_0 is the free space permittivity, ω is the frequency of the light, ε is the complex permittivity of the gold, and $|E|$ is the electric field.

B. Thermal Figures of Merit

Several thermal figures of merit are considered, which are described as follows.

1) The ratio of the maximum temperature rise in the media to the maximum temperature rise in the NFT, $(\Delta T_{\mathrm{medium}})/(\Delta T_{\mathrm{NFT}})$. Here, the temperature rise in the media is considered at the end of 1 ns, while the temperature rise in the NFT is considered at steady state. Since it is desirable to have the maximum temperature rise in the medium with the minimum temperature rise in the NFT, this ratio should be as large as possible.
2) *Thermal Spot Size:* The full width at half maxima of the temperature profile at the recording media. Smaller spot size indicates better localization of the heat within the recording medium.
3) *Thermal Gradient:* Calculated at the location that is at 20 K lower than the peak temperature in the recording medium. It is calculated for both the downtrack and cross-track directions. Higher thermal gradients mean less heat is spread out within the recording medium, giving rise to a better performance of the HAMR system.
4) Normalized peak temperature per incident laser power, $(\Delta T_{\mathrm{medium}})/(P_{\mathrm{incident}})$, which denotes the overall thermal efficiency of the system.

All the thermal figures of merit are calculated considering the steady-state temperature of the NFT and the peak temperature of the recording medium after 1 ns.

V. Comparison Among Different NFT Designs

A. Optical Performance of the Tapered NFTs

The calculated optical coupling efficiency is 2.8% for the E antenna with a straight notch. Fig. 3(a) shows the variation of the coupling efficiency with the angle θ for the NFT designs depicted in Fig. 1(c) and (d), respectively. It is found that increasing the taper angle along the negative θ improves the coupling efficiency to a maximum of 4.5% and then decreases sharply when the angle is increased further. The increase in the coupling efficiency is associated with the change in the resonance condition of the NFT due to its change in geometry. Due to the addition of the taper by modifying the angle θ, the length of the notch becomes different in the top side and the bottom side. For example, at an angle of $\theta = -9°$, which corresponds to a peak in the coupling efficiency shown in Fig. 3(a), the length of the notch at the top is the nominal value of 50 nm, while the length of the notch at the bottom becomes 37 nm. It is known that in plasmonic nanostructures, the length significantly influences the resonance modes that it can support [24]. Hence, the variation of the angle θ gives another means to alter the structure geometry and make it resonant at a particular wavelength. Next the effect of variation of the taper angle, α is studied by keeping the taper angle θ constant at 0°. Fig. 3(b) shows the change of the optical coupling efficiency with the taper angle (α), and it is found that the coupling efficiency rises sharply to 7.1% and then drops off slowly. Unlike the previous case, changing the taper angle α does not cause a change in the length of the notch; rather it alters the width of the notch between the top and the bottom and thus modifies the resonant condition. In addition, at the same time, increasing the angle α widens the base of the notch, which acts as a charge reservoir, and helps

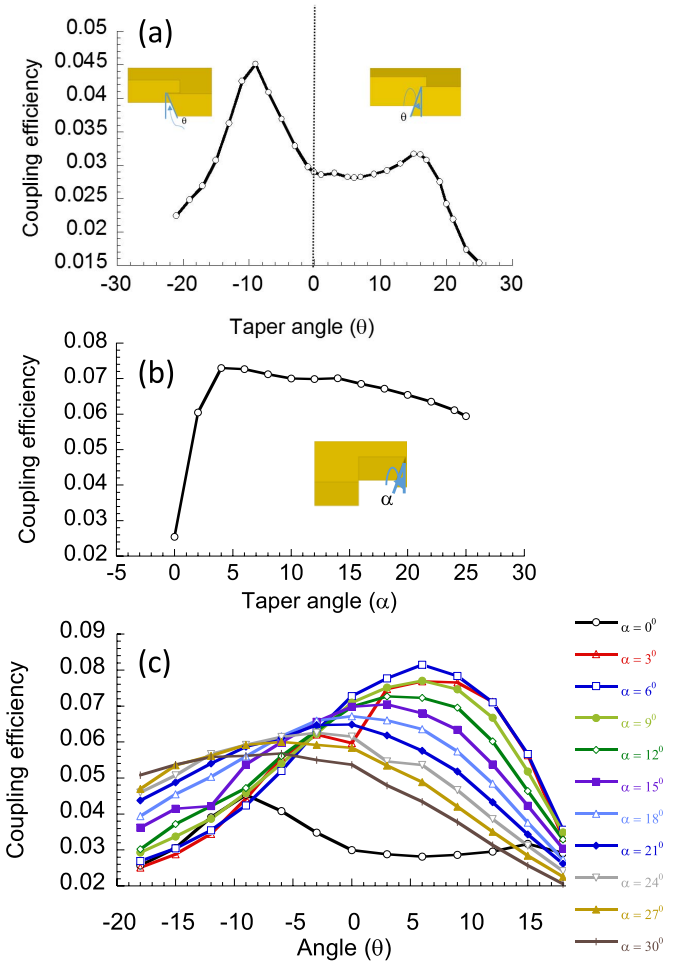

Fig. 3. Coupling efficiency with variation of taper angles (a) for the NFT of Fig. 1(c) and (d), and (b) for the NFT of Fig. 1(e), and (c) θ and α varied simultaneously.

in collecting more charge from the base and funneling it to the tip, thereby increasing the field concentration at the tip of the notch and causing such a sharp rise in the coupling efficiency. However, increasing the taper angle too much affects the Fabry–Perot-type resonance between the top and bottom of the notch, which decreases the coupling efficiency. The effect of varying both taper angles α and θ simultaneously is also studied and the coupling efficiency versus both taper angles is shown in Fig. 3(c). It is seen that with a slight change in α from 0° to 6°, the increase in coupling efficiency is very prominent due to the notch having a wider base. When combined with the modification in θ, we find that with the values of $\alpha = 6°$ and $\theta = 6°$, the coupling efficiency reaches a maximum of 8.1%.

Fig. 4 shows the comparison of the absorption profile in the recording medium and the cross-sectional field intensity for an E antenna with a straight notch and a tapered notch with optimized dimensions of $\alpha = 6°$ and $\theta = 6°$. It is seen from Fig. 4(a) and (b) that the peak absorption in the recording medium is five times higher in the case of the tapered notch. From the cross-sectional views in Fig. 4(c) and (d), it is seen that in the case of the straight notch, there are two hotspots, one at the base of the notch and one at the top of

TABLE I
THERMAL FIGURES OF MERIT FOR E ANTENNA WITH A STRAIGHT NOTCH AND A TAPERED NOTCH

Thermal figures of merit	E antenna with straight notch ($\alpha = 0^0$, $\theta = 0^0$)	E antenna with tapered notch ($\alpha = 6^0$, $\theta = 6^0$)
$\Delta T_{medium} / \Delta T_{NFT}$	1.09	3.07
Thermal spot size at FWHM	150 nm x 81 nm	54 nm x 57 nm
Thermal gradient (measured at 20K temperature difference from the peak temperature in the medium)	2.6 K/nm in cross track 2.5K/nm in down track	7.2 K/nm in cross track 8.5 K/nm in down track
Normalized peak temperature, $\Delta T_{medium} / P_{incident}$	30 K/mW	92.9K/mW

The other key dimensions for both the antennas are a = 316 nm, b = 114 nm, p = 142 nm, q = 300 nm, l = 50 nm, w = 12 nm.

the notch, which are of comparable intensity. On the other hand, having a tapered notch weakens the hotspot at the base of the notch and reduces the charge concentration, which is advantageous to reduce the temperature rise at the base of the notch, which will be discussed in detail in the next section.

B. Comparison of Thermal Performance Between Straight and Tapered E Antenna

A comparative study is presented with respect to the thermal performance of an NFT with a straight notch and an NFT with a tapered notch. The tapered notch has the taper angles of $\alpha = 6°$ and $\theta = 6°$, which gives the maximum coupling efficiency.

Fig. 5(a) and (b) shows the temperature distributions in the recording medium at end of 1 ns for the E antenna with the straight and tapered notches, respectively. Fig. 5(e) shows the temperature rise of the straight and tapered NFTs with respect to time. It is seen that the NFTs reach a steady-state temperature within 200 ns. The temperature of the recording medium rises to 1224 K for the tapered notch compared with 595 K for the straight notch after 1 ns. This increased temperature rise for the tapered notch is primarily due to the increased coupling efficiency of the tapered notch. A greater percentage of the incident power is absorbed in the recording medium leading to a greater rise in temperature.

Fig. 5(c) and (d) shows the temperature profiles in the E antenna with the straight and tapered notches, respectively, at steady state. It is seen that the maximum temperature reaches 568 K for the E antenna with the straight notch, while it is marginally greater, 597 K, for the E antenna with the tapered notch. However, it can be noted that the maximum temperature for the straight notch appears at the bottom of

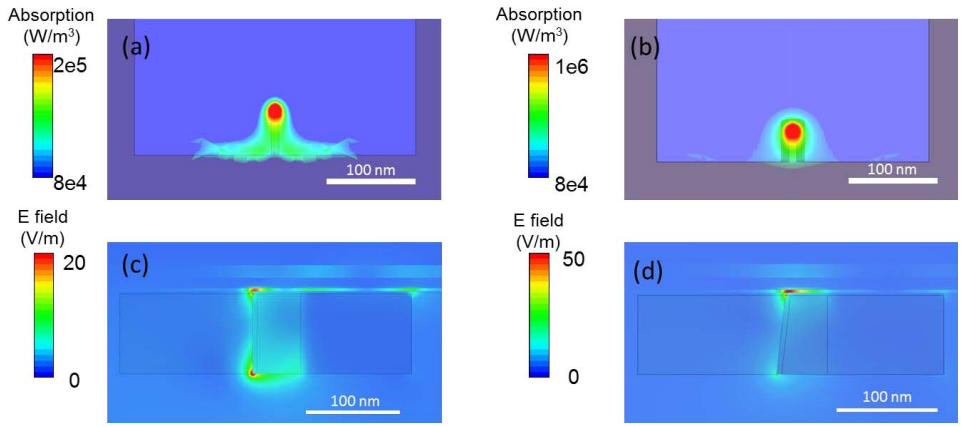

Fig. 4. Absorption profiles in the recording medium for the (a) E antenna with the straight notch and (b) E antenna with the tapered notch. Cross-sectional field plots of the (c) E antenna with the straight notch and (d) E antenna with the tapered notch. The incident electric field for these simulations was 1 V/m. Note that the color bar scales are different in the figure.

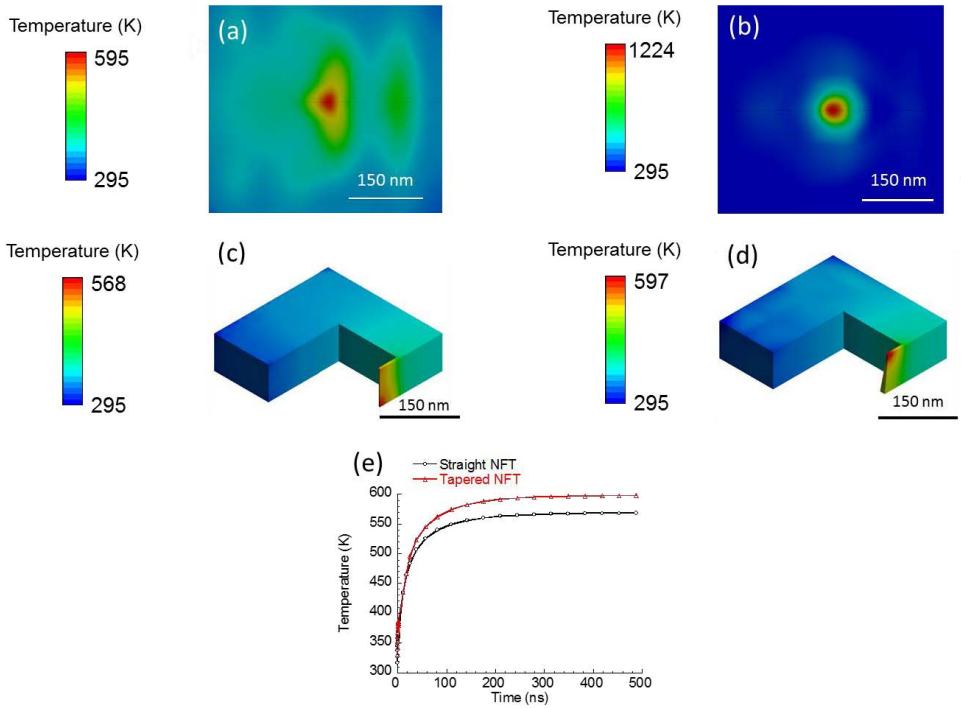

Fig. 5. Temperature field in the recording medium for the (a) E antenna with the straight notch and (b) E antenna with the optimized tapered notch after 1 ns. Temperature fields for NFTs for the (c) E antenna with the straight notch and (d) E antenna with the optimized tapered notch. (e) Temperature increase versus time of the two NFTs.

the notch where the incident laser strikes the NFT. On the other hand, in the case of the tapered notch, the maximum temperature is at the top of the notch, near the ABS of the E antenna. Having a wide base for the tapered notch in the shape of a pyramid helps dissipating the heat from the base of the notch. This pyramidal shape of the notch helps in increasing the conduction path of the notch and acts a better heat sink, which helps in the reduction of the maximum NFT temperature.

Table I summarizes the comparison of various figures of merit for the straight notch and tapered notch E antennas. From the tabular data, it is seen that the tapered notch performs significantly better for all figures of merit. The ratio of the temperature rise in the medium to the NFT is 2.8 times better for the tapered notch, which means that the temperature rise in the tapered notch NFT would be much smaller in order to raise the temperature of the recording medium to a particular value. The thermal spot size is 54 nm $\times$ 57 nm for the tapered notch, whereas the spot size is 150 nm $\times$ 81 nm for a straight notch of similar notch dimensions. Similarly, the thermal gradient in the recording medium is about three times higher for the tapered notch in both cross- and downtrack directions, which ensures lower thermal tail. Finally, for the straight notch NFT, the temperature of the medium increases by 30 K/mW of

incident laser power, while it is about 93 K/mW for the tapered notch NFT. Hence, a lower power laser would be sufficient to raise the temperature of the recording medium to the desired value.

VI. Conclusion

We studied the effect of introducing tapers in the design of an E-shaped NFT. It was found that with proper modification of the notch of an E antenna, the optical coupling efficiency can be improved over the existing design. The greatest advantage comes in the thermal figures of merit. A tapered notch with a wide base acts as a form of a heat sink and the thermal performance of such an NFT is several times better in terms of thermal figures of merit. This gives us a new strategy for designing more efficient and functional NFTs for the next-generation HAMR applications.

Acknowledgment

This work was supported in part by the National Science Foundation and in part by the Advanced Storage Technology Consortium (ASTC).

References

[1] EMC. (Apr. 9, 2014). *Digital Universe Invaded By Sensors*. [Online]. Available: http://www.emc.com/about/news/press/2014/20140409-01.htm

[2] N. Zhou *et al.*, "Plasmonic near-field transducer for heat-assisted magnetic recording," *Nanophotonics*, vol. 3, no. 3, pp. 141–155, 2014.

[3] R. E. Rottmayer *et al.*, "Heat-assisted magnetic recording," *IEEE Trans. Magn.*, vol. 42, no. 10, pp. 2417–2421, Oct. 2006.

[4] M. H. Kryder *et al.*, "Heat assisted magnetic recording," *Proc. IEEE*, vol. 96, no. 11, pp. 1810–1835, Nov. 2008.

[5] J. A. Schuller, E. S. Barnard, W. Cai, Y. C. Jun, J. S. White, and M. L. Brongersma, "Plasmonics for extreme light concentration and manipulation," *Nature Mater.*, vol. 9, pp. 193–204, Feb. 2010.

[6] L. Novotny and N. Van Hulst, "Antennas for light," *Nature Photon.*, vol. 5, pp. 83–90, Feb. 2011.

[7] D. Weller and A. Moser, "Thermal effect limits in ultrahigh-density magnetic recording," *IEEE Trans. Magn.*, vol. 35, no. 6, pp. 4423–4439, Nov. 1999.

[8] W. A. Challener and A. V. Itagi, "Near-field optics for heat-assisted magnetic recording (experiment, theory, and modeling)," in *Modern Aspects of Electrochemistry No. 44*. New York, NY, USA: Springer, 2009, pp. 53–111.

[9] B. C. Stipe *et al.*, "Magnetic recording at 1.5 Pb m^{-2} using an integrated plasmonic antenna," *Nature Photon.*, vol. 4, pp. 484–488, May 2010.

[10] W. A. Challener *et al.*, "Heat-assisted magnetic recording by a near-field transducer with efficient optical energy transfer," *Nature Photon.*, vol. 3, no. 4, pp. 220–224, 2009.

[11] N. Zhou, L. M. Traverso, and X. Xu, "Power delivery and self-heating in nanoscale near field transducer for heat-assisted magnetic recording," *Nanotechnology*, vol. 26, no. 13, p. 134001, 2015.

[12] X. Shi and L. Hesselink, "Mechanisms for enhancing power throughput from planar nano-apertures for near-field optical data storage," *Jpn. J. Appl. Phys.*, vol. 41, no. 3B, p. 1632, 2002.

[13] T. Matsumoto, F. Akagi, M. Mochizuki, H. Miyamoto, and B. Stipe, "Integrated head design using a nanobeak antenna for thermally assisted magnetic recording," *Opt. Exp.*, vol. 20, no. 17, pp. 18946–18954, 2012.

[14] S. P. Powell, E. J. Black, T. E. Schlesinger, and J. A. Bain, "The influence of media optical properties on the efficiency of optical power delivery for heat assisted magnetic recording," *J. Appl. Phys.*, vol. 109, no. 7, p. 07B775, 2011.

[15] B. X. Xu *et al.*, "Thermal issues and their effects on heat-assisted magnetic recording system," *J. Appl. Phys.*, vol. 111, no. 7, p. 07B701, 2012.

[16] S. Bhargava and E. Yablonovitch, "Lowering HAMR near-field transducer temperature via inverse electromagnetic design," *IEEE Trans. Magn.*, vol. 51, no. 4, Apr. 2015, Art. no. 3100407.

[17] Y. Chen, J. Chen, X. Xu, and J. Chu, "Fabrication of bowtie aperture antennas for producing sub-20 nm optical spots," *Opt. Exp.*, vol. 23, no. 7, pp. 9093–9099, 2015.

[18] P. B. Johnson and R. W. Christy, "Optical constants of the noble metals," *Phys. Rev. B*, vol. 6, p. 4370, Dec. 1972.

[19] Y. Wang, T. Maletzky, E. X. Jin, D. Zhou, J. Smyth, and M. Dovek, "Pulsed thermally assisted magnetic recording," *IEEE Trans. Magn.*, vol. 49, no. 2, pp. 739–743, Feb. 2013.

[20] B. X. Xu *et al.*, "Performance benefits from pulsed laser heating in heat assisted magnetic recording," *J. Appl. Phys.*, vol. 115, no. 17, p. 17B701, 2014.

[21] N. Zuckerman and J. Fang, "Two carrier heat transfer modeling for heat assisted magnetic recording," in *Proc. ASME Heat Transf. Summer Conf. Collocated ASME 7th Int. Conf. Energy Sustainab. ASME 11th Int. Conf. Fuel Cell Sci., Eng. Technol.*, 2013, p. V001T03A006.

[22] H. Li, M. Kurita, J. Xu, and S. Yoshida, "Iteration method for analysis of write-current-induced thermal protrusion," *Microsyst. Technol.*, vol. 16, pp. 161–167, Jan. 2010.

[23] P. Yu, W. Zhou, S. Yu, and Y. Zeng, "Laser-induced local heating and lubricant depletion in heat assisted magnetic recording systems," *Int. J. Heat Mass Transf.*, vol. 59, pp. 36–45, Apr. 2013.

[24] J. Dorfmüller *et al.*, "Fabry–Pérot resonances in one-dimensional plasmonic nanostructures," *Nano Lett.*, vol. 9, no. 6, pp. 2372–2377, 2009.